# Topological Nodal-Net Semimetal in a Graphene Network Structure

Jian-Tao Wang,[1,2,*] Simin Nie,[1] Hongming Weng,[1,3] Yoshiyuki Kawazoe,[4] and Changfeng Chen[5]
[1]*Beijing National Laboratory for Condensed Matter Physics, Institute of Physics, Chinese Academy of Sciences, Beijing 100190, China*
[2]*School of Physics, University of Chinese Academy of Sciences, Beijing 100049, China*
[3]*Collaborative Innovation Center of Quantum Matter, Beijing 100190, China*
[4]*New Industry Creation Hatchery Center, Tohoku University, Sendai 980-8579, Japan*
[5]*Department of Physics and High Pressure Science and Engineering Center, University of Nevada, Las Vegas, Nevada 89154, USA*

(Received 8 March 2017; revised manuscript received 12 November 2017; published 12 January 2018)

Topological semimetals are characterized by the nodal points in their electronic structure near the Fermi level, either discrete or forming a continuous line or ring, which are responsible for exotic properties related to the topology of bulk bands. Here we identify by *ab initio* calculations a distinct topological semimetal that exhibits nodal nets comprising multiple interconnected nodal lines in bulk and have two coupled drumheadlike flat bands around the Fermi level on its surface. This nodal net semimetal state is proposed to be realized in a graphene network structure that can be constructed by inserting a benzene ring into each C—C bond in the bct-$C_4$ lattice or by a crystalline modification of the (5,5) carbon nanotube. These results expand the realm of nodal manifolds in topological semimetals, offering a new platform for exploring novel physics in these fascinating materials.

DOI: 10.1103/PhysRevLett.120.026402

The valence electrons of a carbon atom can form $sp^3$-, $sp^2$-, and $sp$-hybridized states that support single, double, triple, and aromatic C—C bonds [1–3], which profoundly impact a wide range of properties of carbon-based materials [4–10]. At ambient conditions, graphite is the most stable carbon phase; its honeycomb lattice can be viewed as a planar molecule comprising benzene rings in an all-$sp^2$ bonding state, which hosts a semimetallic electronic structure. At high pressures, graphite can be converted into insulating cubic or hexagonal diamond at high temperatures [11–14] or, under cold compression, into all-$sp^3$ diamondlike [15–21] or $sp^2$-$sp^3$ hybrid diamond-graphite carbon forms [22]. The graphitic sheet can also be peeled off or wrapped into new structural forms such as fullerenes [23], nanotubes [24], and graphene [25]. Experimental studies [26–29] have identified a transformation of compressed carbon nanotube (CNT) to diamond. Recently, with the assistance of computational design, a porous aromatic carbon framework structure constructed by inserting a phenyl ring into each C—C bond of the diamond lattice has been synthesized [30]; moreover, 3D conductive interconnected graphene networks have been synthesized by chemical vapor deposition [31]. Meanwhile, several theoretical studies have predicted a number of carbon-network topological nodal line semimetals in all-$sp^2$ or $sp^2$-$sp^3$ hybrid networks [32–37]. These advances open exciting avenues for constructing additional carbon network structures with outstanding properties.

In this Letter, we report *ab initio* calculations [38–43] that identify a new body-centered tetragonal carbon allotrope in $I4/mmm$ ($D_{4h}^{17}$) symmetry, which can be constructed by inserting a benzene ring into each C—C bond in a previously established bct-$C_4$ carbon lattice [17], or by a structural modification of the (5,5) CNT. The resulted interconnected graphene network structure contains forty atoms in one unit cell, thus termed bct-$C_{40}$. Electronic band structure calculations reveal a novel topological semimetallic state in bct-$C_{40}$, which is distinct from the known nodal-point semimetals [44] and the more recently intensively studied nodal-line semimetals [45–59]. The electronic structure of bct-$C_{40}$ possesses two mirror symmetric boxed-asterisk shaped nodal nets comprising interconnected nodal lines. The nodal lines all go through the whole Brillouin zone (BZ), leading to a netlike structure. Calculations also show two coupled drumhead surface flat bands [34] around the Fermi level bounded by the projection of the bulk nodal lines on surface. The complex nodal-manifold structure and the multiple coupled surface flat bands place bct-$C_{40}$ into a new class of topological nodal-net semimetal. Our findings expand the realm of topological semimetals in their characteristic nodal structures, and these results offer new opportunities to explore the remarkable properties of these novel materials.

Our calculations are carried out using the density functional theory as implemented in the Vienna *ab initio* simulation package (VASP) [38]. The generalized gradient approximation (GGA) developed by Armiento-Mattsson (AM05) [39] was adopted for the exchange-correlation

 

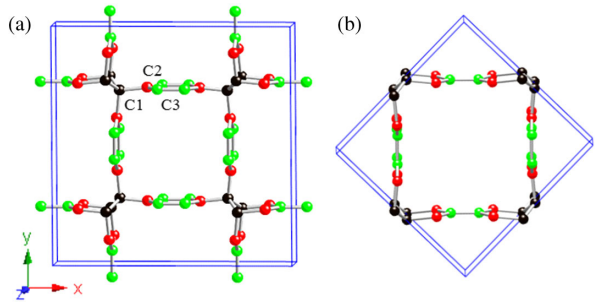


FIG. 1. (a) The 40-atom unit cell of bct-$C_{40}$ with lattice parameters a = 12.9012 Å, $c = 2.4599$ Å, occupying the $8h$ (0.7257, 0.7257, 0.5), $16l_1$ (0.7370, 0.6096, 0.5), and $16l_2$ (0.7615, 0.0558, 0.5) Wyckoff positions denoted by $C_1$, $C_2$ and $C_3$, respectively. (b) A 20-atom primitive cell of bct-$C_{40}$ viewed as a crystalline modification of the (5,5) CNT.

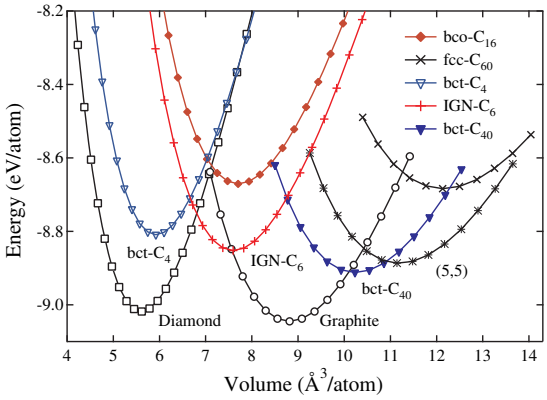


FIG. 2. Calculated energies vs volume per atom for bct-$C_{40}$ compared to graphite, fcc-$C_{60}$ [60], bco-$C_{16}$ [35], (5,5) CNT, bct-$C_4$ [17], diamond, and IGN-$C_6$ [32].

function for the structural relaxation. The all-electron projector augmented wave (PAW) method [40] was adopted with $2s^2 2p^2$ treated as valence electrons. A plane-wave basis set with a large energy cutoff of 800 eV was used. Convergence criteria employed for both the electronic self-consistent relaxation and the ionic relaxation were set to $10^{-8}$ eV and 0.01 eV/Å for energy and force, respectively. The electronic band structures and related properties are obtained using the standard GGA-PBE method [41], while the band gaps are corrected using a hybrid density functional based on the Heyd-Scuseria-Ernzerhof scheme (HSE06) [42]. Phonon calculations are performed using the phonopy code [43].

Figure 1(a) shows the body-centered tetragonal interpenetrated graphene network structure of bct-$C_{40}$ in $I4/mmm$ ($D_{4h}^{17}$) symmetry. The calculated equilibrium lattice parameters are $a = 12.901$ Å and $c = 2.46$ Å with three inequivalent crystallographic sites $C_1$, $C_2$, and $C_3$, occupying the $8h$ (0.7257, 0.7257, 0.5), $16l_1$ (0.7370, 0.6096, 0.5), and $16l_2$ (0.7615, 0.0558, 0.5) Wyckoff positions, respectively. The carbon atoms on the $16l_1$ and $16l_2$ sites form eight benzene rings with aromatic $sp^2$ hybridization, while the carbon atoms on the $8h$ sites form four zigzag carbon chains as in bct-$C_4$. There are two sets of distinct C—C bonds in this structure, namely, two $sp^3$ single longer bonds of 1.516 ($C_1$—$C_1$) and 1.505 Å ($C_1$—$C_2$), and two shorter $sp^2$ aromatic bonds of 1.412 ($C_2$—$C_3$) and 1.440 Å ($C_3$—$C_3$). There are also two sets of distinct bond angles: 109.49° for $\angle C_1$—$C_1$—$C_1$, 111.80° for $\angle C_1$—$C_1$—$C_2$, and 101.09° for $\angle C_2$—$C_1$—$C_2$, which are close to the 109.5° angle in diamond; 119.37° for $\angle C_1$—$C_2$—$C_3$, 121.11° for $\angle C_3$—$C_2$—$C_3$, and 119.43° for $\angle C_3$—$C_3$—$C_2$, which are close to the 120° angle in graphene. Note that bct-$C_{40}$ has a 20-atom primitive cell [see Fig. 1(b)], and it can be regarded as a crystalline modification of (5,5) CNT [29], similar to the case of bct-$C_4$ being viewed as a polymerized form of the (2,2) CNT [17].

We show in Fig. 2 the total energy per atom as a function of volume for bct-$C_{40}$ compared with the results for diamond, graphite, fcc-$C_{60}$ fullerene [60], interpenetrated graphene network IGN-$C_6$ [32], bco-$C_{16}$ [35], bct-$C_4$ [17], and the (5,5) CNT. The calculated energetic data establish the following stability sequence: $C_{60} \simeq$ bco-$C_{16}$ < bct-$C_4$ < IGN-$C_6$ < (5,5) < bct-$C_{40}$ < diamond < graphite. While bct-$C_{40}$ is slightly (0.11 − 0.13 eV/atom) higher in energy than diamond and graphite, it is more stable than all the other carbon phases examined here. The equilibrium volume of bct-$C_{40}$ is between those of graphite and the (5,5)-CNT. These energetic and volume data suggest possible synthesis of bct-$C_{40}$ by compressing CNT [29]. By fitting the calculated total energy as a function of volume to Murnaghan's equation of state [61], we obtain the bulk modulus ($B_0$) of 239 GPa for bct-$C_{40}$, which is smaller than 280 GPa for graphite due to the lower atomic density (see Table I).

We have also calculated the phonon band structure of bct-$C_{40}$ at zero pressure and found no imaginary frequency modes in the entire BZ (see Supplemental Material [62], Fig. S1), thus confirming its dynamical stability. We further evaluated the phonon contributions to the Helmholtz free energy using the quasi-harmonic approximation [63]. The calculated Helmholtz free energies (see Fig. S2) show that bct-$C_{40}$ is less stable than diamond and graphite, but more stable than bco-$C_{16}$, fcc-$C_{60}$, bct-$C_4$, IGN-$C_6$, and (5,5) CNT, over a wide temperature range from 0 to 1600 K, confirming bct-$C_{40}$ as a viable thermodynamically stable phase.

Having established the structural viability of bct-$C_{40}$, we explore its topological semimetal states that have been proposed to exist in graphenelike structures and been found to be sensitive to the configuration and connectivity of graphene network structures [32]. Our electronic band structure calculations reveal that bct-$C_{40}$ has interconnected nodal lines forming two nearly two-dimensional nodal nets in BZ [Figs. 3(b), 3(c)], which is distinct from all existing, both nodal point and nodal line, topological semimetals [69]. The crossing bands forming these nodal lines belong to two different irreducible representations $G_1$ and $G_2$ [Fig. 3(a)] distinguished by opposite mirror eigenvalues.

TABLE I. Calculated equilibrium structural parameters (space group, lattice parameters $a$, $b$, and $c$, bond lengths $d_{C-C}$), density $\rho$, total energy $E_{tot}$, bulk modulus $B_0$, and HSE06 electronic band gap $E_g$ for bct-$C_{40}$ along with results for diamond, bct-$C_4$ [17], bco-$C_{16}$ [35], IGN-$C_6$ [32], and graphite at zero pressure, compared to available experimental data [11].

| Structure | Method | $\rho(g/cm^3)$ | $a$ (Å) | $b$ (Å) | $c$ (Å) | $d_{C-C}$ (Å) | $E_{tot}$ (eV) | $B_0$ (GPa) | $E_g$ (eV) |
|---|---|---|---|---|---|---|---|---|---|
| Diamond ($Fd\bar{3}m$) | AM05 | 3.56 | 3.552 | | | 1.538 | −9.018 | 451 | 5.36 |
| | Exp [11] | 3.52 | 3.567 | | | 1.544 | | 446 | 5.47 |
| bct-$C_4$ ($I4/mmm$) | AM05 [17] | 3.37 | 4.354 | | 2.498 | 1.516, 1.570 | −8.809 | 419 | 3.42 |
| bco-$C_{16}$ ($Imma$) | AM05 [35] | 2.59 | 7.806 | 4.877 | 3.237 | 1.382–1.459 | −8.671 | 315 | Semimetal |
| ign-$C_6$ ($Cmcm$) | AM05 [32] | 2.63 | 5.899 | 6.281 | 2.459 | 1.406–1.522 | −8.852 | 323 | Semimetal |
| bct-$C_{40}$ ($I4/mmm$) | AM05 | 1.95 | 12.901 | | 2.460 | 1.412–1.516 | −8.912 | 239 | Semimetal |
| Graphite ($P6_3/mmc$) | AM05 | 2.27 | 2.462 | | 6.710 | 1.422 | −9.045 | 280 | Semimetal |
| | Exp [11] | 2.27 | 2.460 | | 6.704 | 1.420 | | 286 | |

The resulted nodal lines go through the whole BZ instead of forming a closed ring inside BZ [64]. They are topologically robust protected by the coexisting time-reversal and inversion symmetries without considering the spin-orbit coupling [34] and are constrained on the mirror planes [70]. They form two boxed-asterisk shaped nets and the connecting points are on the intersecting lines of different mirror planes, which are similar to those in other nodal chain semimetals [65–67]. It is noted that the spin-orbit coupling may open up a gap at all of the band crossing points, but the extremely weak (0.13–0.74 meV) coupling strength in carbon [34–36] is not expected to alter the semimetallic features in bct-$C_{40}$ with both electron and hole pockets. To test the robustness of these results, we have also calculated the electronic band structures using the hybrid density functional HSE06 method [42] along the high-symmetry direction of $G$-$L$-$X$ (see Supplemental Material [62], Fig. S3). The results show that both the band crossing feature from the $G_1$ and $G_2$ bands and the nodal points obtained using the GGA-PBE functional are well preserved.

When the resulted nodal nets are projected onto the surface BZ, there might have been topologically protected surface flat bands. Figure 4 shows the calculated (110) [Figs. 4(a), 4(b)] and (100) [Figs. 4(c), 4(d)] surface states of bct-$C_{40}$ using an eight-layer and ten-layer thick slab geometry along the [110] and [100] crystalline directions, respectively (see the slab geometries in the Supplemental Material [62], Fig. S4). The projections of one nodal net on to the (110) and (100) planes are shown in Figs. 4(e) and 4(f), respectively. The numbers indicate the corresponding bulk nodal lines as labeled in Fig. 3(c). The top and bottom surface bands are marked in red solid and green dotted lines, respectively. They are degenerate due to the inversion symmetric slab model used in the calculation. The surface bands can be inside (region containing the $\bar{G}$ point) or outside (region containing the BZ boundaries) of the momentum space divided by the two symmetric nodal nets depending on the details of the surface termination. When the surface dangling bonds are (not) saturated with hydrogen atoms, the surface bands are outside (inside), which are similar to the results obtained in other nodal line systems [35,49]. A distinct property of bct-$C_{40}$ is that it hosts two surface flat bands, which is different from the previously proposed nodal line semimetals with only a single flat surface band inside or outside the projected nodal line or ring [32–35]. This distinct property is due to

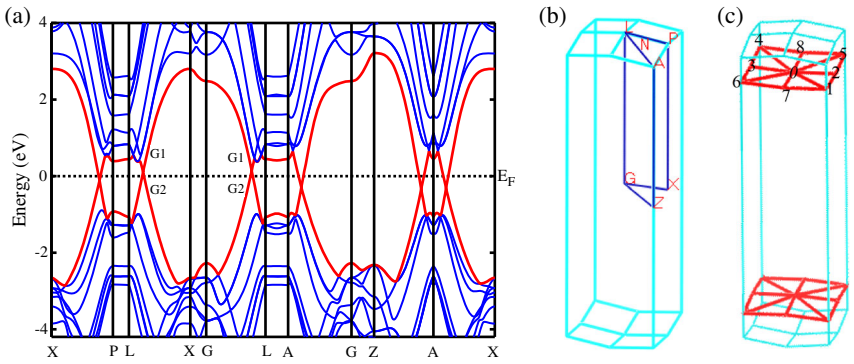


FIG. 3. Calculated bulk electronic band structures of bct-$C_{40}$ at equilibrium lattice parameters using the standard GGA-PBE functional. (a) The results along several high-symmetry directions. $G_1$ and $G_2$ indicate the irreducible representations of the two crossing bands, respectively. (b) The bulk Brillouin zone with several high-symmetry points indicated at $G$(0.00, 0.00, 0.00); $X$(0.00, 0.00, 0.50); $P$(0.25, 0.25, 0.25); $N$(0.00, 0.50, 0.00); $Z$(−0.50, 0.50, 0.50); $L$(0.26, 0.26, −0.26), and $A$(−0.26, 0.74, 0.26). (c) Two symmetric boxed-asterisk shaped nodal nets consisting of six nodal lines of 3-0-2, 7-0-8, 6-7-1, 1-2-5, 6-0-5, and 4-0-1, which link the high-symmetry nodal points 0 (0.192, 0.192, −0.192), 1 (−0.301, 0.699, 0.301), 2 (0.195, 0.195, 0.305), and others (points 3 through 8) that are generated from points 0, 1, and 2 by symmetry operations.

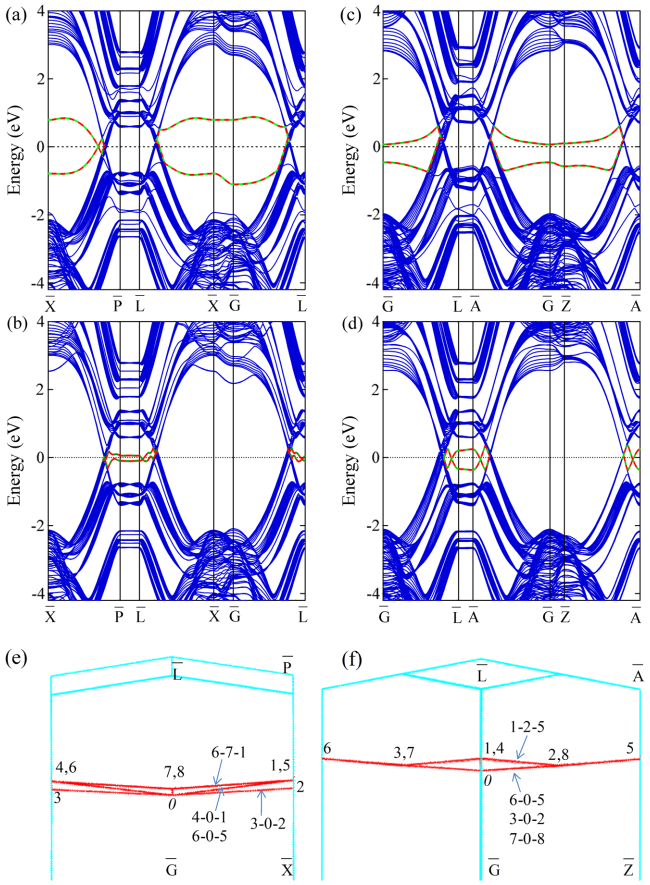


FIG. 4. Calculated surface band structures of bct-$C_{40}$ using the standard GGA-PBE functional. (a,b) The (110) surface states obtained using an eight-layer-thick slab geometry along the [110] direction; (c,d) The (100) surface states obtained using a ten-layer-thick slab geometry along the [100] direction. In (b,d) the surface dangling bonds are saturated with hydrogen atoms. The surface bands are marked in red solid and green dot lines. (e,f) The projected nodal lines on the $\bar{X}$-$\bar{P}$-$\bar{L}$-$\bar{G}$ (110) and $\bar{Z}$-$\bar{A}$-$\bar{L}$-$\bar{G}$ (100) planes of the bulk Brillouin zone, corresponding to the projected surface Brillouin zones of the (110) and (100) planes in (a–d).

the superposition of the projection regions from the multiple nodal lines in the nodal net. Recently, Hyart *et al.* [64,67] and Bzdusek *et al.* [65] have studied this situation and found that it is possible to have multiple zero-energy flat surface bands if chiral symmetry is assumed. In the case of bct-$C_{40}$, the chiral symmetry is absent, and the coupling of the two surface states opens a gap with two bands located below and above the Fermi level, respectively. The surface states predicted for the nodal net semimetals should be detectable by photoelectron spectroscopy [56] and provide a multiband, instead of single-band, platform for exploring novel phenomena associated with correlated physics based on topological nodal line semimetals, such as possible higher-temperature superconductivity [50], chiral superconductivity with spontaneous time-reversal symmetry broking, gapless Pomeranchuk phase with spontaneous rotation symmetry broking, and gapped insulating phase with spontaneous mirror symmetry broking [71].

In summary, we have identified by *ab initio* calculations a body-centered-tetragonal interconnected graphene network structure bct-$C_{40}$. This new carbon phase can be characterized as and possibly synthesized by a crystalline modification of the (5,5) carbon nanotube through compression [29]. Electronic band structure calculations reveal that bct-$C_{40}$ belongs to a new class of topological nodal net semimetal and possesses two nearly two-dimentional boxed-asterisk shaped nodal-line nets related by inversion symmetry or time-reversal symmetry. When the nodal lines consisting of the nodal nets are projected onto surfaces, the projection regions are superposed and our calculations show two coupled surface flat bands with one occupied and the other unoccupied. This finding provides a multiband rather than a single-band based flat-band platform to study possible novel correlated effects, such as flat-band driven high-temperature superconductivity, chiral superconductivity, and more.

This study was supported by the National Natural Science Foundation of China (Grants No. 11674364 and No. 11674369) and the Strategic Priority Research Program of the Chinese Academy of Sciences (Grant No. XDB07000000). H. W. acknowledges the support from the National Key Research and Development Program of China (Grant No. 2016YFA0300600). C. F. C. acknowledges support by DOE under Cooperative Agreement No. DE-NA0001982.

*Note added.*—Recently, several works have reported advances in unveiling the topology of nodal lines. Further discussions in the context of recent developments are given in the Supplemental Material [62].

*wjt@aphy.iphy.ac.cn

[1] W. A. Chalifoux and R. R. Tykwinski, Nat. Chem. **2**, 967 (2010).
[2] J. T. Wang, C. F. Chen, and Y. Kawazoe, Sci. Rep. **3**, 3077 (2013).
[3] E. A. Belenkov and V. A. Greshnyakov, Phys. Solid State **55**, 1754 (2013).
[4] J. T. Wang, C. F. Chen, E. G. Wang, and Y. Kawazoe, Sci. Rep. **4**, 4339 (2014).
[5] R. H. Baughman, H. Eckhardt, and M. Kertesz, J. Chem. Phys. **87**, 6687 (1987).
[6] J. T. Wang, C. F. Chen, H. D. Li, H. Mizuseki, and Y. Kawazoe, Sci. Rep. **6**, 24665 (2016).
[7] A. San-Miguel and P. Toulemonde, High Press. Res. **25**, 159 (2005).
[8] N. Rey, A. Munoz, P. Rodríguez-Hernández, and A. San-Miguel, J. Phys. Condens. Matter **20**, 215218 (2008).
[9] J. T. Wang, C. F. Chen, D. S. Wang, H. Mizuseki, and Y. Kawazoe, J. Appl. Phys. **107**, 063507 (2010).
[10] H. A. Calderon, I. Estrada-Guel, F. Alvarez-Ramirez, V. G. Hadjiev, and F. C. Robles-Hernandez, Carbon **102**, 288 (2016).
[11] F. Occelli, P. Loubeyre, and R. Letoullec, Nat. Mater. **2**, 151 (2003).
[12] R. Clarke and C. Uher, Adv. Phys. **33**, 469 (1984).

[13] I. Irifune, A. Kurio, S. Sakamoto, T. Inoue, and H. Sumiya, Nature (London) **421**, 599 (2003).
[14] P. Németh, L. A. J. Garvie, T. Aoki, N. Dubrovinskaia, L. Dubrovinsky, and P. R. Buseck, Nat. Commun. **5**, 5447 (2014).
[15] W. L. Mao, H. K. Mao, P. J. Eng, T. P. Trainor, M. Newville, C. C. Kao, D. L. Heinz, J. F. Shu, Y. Meng, and R. J. Hemley, Science **302**, 425 (2003).
[16] H. Y. Niu, X. Q. Chen, S. B. Wang, D. Z. Li, W. L. Mao, and Y. Y. Li, Phys. Rev. Lett. **108**, 135501 (2012).
[17] K. Umemoto, R. M. Wentzcovitch, S. Saito, and T. Miyake, Phys. Rev. Lett. **104**, 125504 (2010).
[18] Q. Li, Y. M. Ma, A. R. Oganov, H. B. Wang, H. Wang, Y. Xu, T. Cui, H. K. Mao, and G. T. Zou, Phys. Rev. Lett. **102**, 175506 (2009).
[19] J. T. Wang, C. F. Chen, and Y. Kawazoe, Phys. Rev. Lett. **106**, 075501 (2011).
[20] M. Amsler, J. A. Flores-Livas, L. Lehtovaara, F. Balima, S. A. Ghasemi, D. Machon, S. Pailhes, A. Willand, D. Caliste, S. Botti, A. San Miguel, S. Goedecker, and M. A. L. Marques, Phys. Rev. Lett. **108**, 065501 (2012).
[21] Z. S. Zhao, F. Tian, X. Dong, Q. Li, Q. Q. Wang, H. Wang, X. Zhong, B. Xu, D. L. Yu, J. L. He, H. T. Wang, Y. M. Ma, and Y. J. Tian, J. Am. Chem. Soc. **134**, 12362 (2012).
[22] F. J. Ribeiro, S. G. Louie, M. L. Cohen, and P. Tangney, Phys. Rev. B **72**, 214109 (2005).
[23] H. W. Kroto, J. R. Heath, S. C. Obrien, R. F. Curl, and R. E. Smaliey, Nature (London) **318**, 162 (1985).
[24] S. Iijima, Nature (London) **354**, 56 (1991).
[25] K. S. Novoselov, A. K. Geim, S. V. Morozov, D. Jiang, Y. Zhang, S. V. Dubonos, I. V. Grigorieva, and A. A. Firsov, Science **306**, 666 (2004).
[26] V. N. Khabashesku, Z. N. Gu, B. Brinson, J. L. Zimmerman, J. L. Margrave, V. A. Davydov, L. S. Kashevarova, and A. V. Rakhmanina, J. Phys. Chem. B **106**, 11155 (2002).
[27] Z. W. Wang, Y. S. Zhao, K. Tait, X. Z. Liao, D. Schiferl, C. S. Zha, R. T. Downs, J. Qian, Y. T. Zhu, and T. D. Shen, Proc. Natl. Acad. Sci. U.S.A. **101**, 13699 (2004).
[28] A. Merlen, P. Toulemonde, S. L. Floch, G. Montagnac, T. Hammouda, O. Marty, and A. S. Miguel, Carbon **47**, 1643 (2009).
[29] A. Kuc and G. Seifert, Phys. Rev. B **74**, 214104 (2006).
[30] T. Ben, H. Ren, S. Q. Ma, D. P. Cao, J. H. Lan, X. F. Jing, W. C. Wang, J. Xu, F. Deng, J. M. Simmons, S. L. Qiu, and G. S. Zhu, Angew. Chem., Int. Ed. **48**, 9457 (2009).
[31] Z. Chen, W. Ren, L. Gao, B. Liu, S. Pei, and H. Cheng, Nat. Mater. **10**, 424 (2011).
[32] Y. P. Chen, Y. E. Xie, S. A. Yang, H. Pan, F. Zhang, M. L. Cohen, and S. B. Zhang, Nano Lett. **15**, 6974 (2015).
[33] K. Mullen, B. Uchoa, and D. T. Glatzhofer, Phys. Rev. Lett. **115**, 026403 (2015).
[34] H. Weng, Y. Liang, Q. Xu, R. Yu, Z. Fang, X. Dai, and Y. Kawazoe, Phys. Rev. B **92**, 045108 (2015).
[35] J. T. Wang, H. Weng, S. M. Nie, Z. Fang, Y. Kawazoe, and C. F. Chen, Phys. Rev. Lett. **116**, 195501 (2016).
[36] Y. Cheng, J. Du, R. Melnik, Y. Kawazoe, and B. Wen, Carbon **98**, 468 (2016).
[37] G. P. Mikitik and Y. V. Sharlai, Phys. Rev. B **73**, 235112 (2006).
[38] G. Kresse and J. Furthmüller, Phys. Rev. B **54**, 11169 (1996).
[39] R. Armiento and A. E. Mattsson, Phys. Rev. B **72**, 085108 (2005).
[40] P. E. Blöchl, Phys. Rev. B **50**, 17953 (1994).
[41] J. P. Perdew, K. Burke, and M. Ernzerhof, Phys. Rev. Lett. **77**, 3865 (1996).
[42] J. Heyd, G. E. Scuseria, and M. Ernzerhof, J. Chem. Phys. **124**, 219906 (2006).
[43] A. Togo, F. Oba, and I. Tanaka, Phys. Rev. B **78**, 134106 (2008).
[44] N. P. Armitage, E. J. Mele, and Ashvin Vishwanath, arXiv:1705.01111 [Rev. Mod. Phys. (to be published)].
[45] A. A. Burkov, M. D. Hook, and L. Balents, Phys. Rev. B **84**, 235126 (2011).
[46] M. Phillips and V. Aji, Phys. Rev. B **90**, 115111 (2014).
[47] C. Fang, Y. Chen, H. Y. Kee, and L. Fu, Phys. Rev. B **92**, 081201 (2015).
[48] Y. Kim, B. J. Wieder, C. L. Kane, and A. M. Rappe, Phys. Rev. Lett. **115**, 036806 (2015).
[49] R. Yu, H. Weng, Z. Fang, X. Dai, and X. Hu, Phys. Rev. Lett. **115**, 036807 (2015).
[50] G. E. Volovik, Phys. Scr. **T164**, 014014 (2015).
[51] T. T. Heikkila and G. E. Volovik, New J. Phys. **17**, 093019 (2015).
[52] L. S. Xie, L. M. Schoop, E. M. Seibel, Q. D. Gibson, W. Xie, and R. J. Cava, APL Mater. **3**, 083602 (2015).
[53] Y.-H. Chan, C.-K. Chiu, M. Y. Chou, and A. P. Schnyder, Phys. Rev. B **93**, 205132 (2016).
[54] Z. Yan and Z. Wang, Phys. Rev. Lett. **117**, 087402 (2016).
[55] C.-K. Chan, Y.-T. Oh, J. H. Han, and P. A. Lee, Phys. Rev. B **94**, 121106 (2016).
[56] G. Bian *et al.*, Nat. Commun. **7**, 10556 (2016).
[57] C. L. Zhang, Z. J. Yuan, G. Bian, S. Y. Xu, X. Zhang, M. Z. Hasan, and S. Jia, Phys. Rev. B **93**, 054520 (2016).
[58] M. Ezawa, Phys. Rev. Lett. **116**, 127202 (2016).
[59] X. M. Zhang, Z. M. Yu, X. L. Sheng, H. Y. Yang, and S. A. Yang, Phys. Rev. B **95**, 235116 (2017).
[60] W. I. F. David, R. M. Ibberson, J. C. Matthewman, K. Prassides, T. J. S. Dennis, J. P. Hare, H. W. Kroto, R. Taylor, and D. R. M. Walton, Nature (London) **353**, 147 (1991).
[61] F. D. Murnaghan, Proc. Natl. Acad. Sci. U.S.A. **30**, 244 (1944).
[62] See Supplemental Material at http://link.aps.org/supplemental/10.1103/PhysRevLett.120.026402 for calculated phonon dispersion and density of states (Fig. S1); Helmholtz free energies (Fig. S2); HSE06 electronic band structures (Fig. S3); geometries of an eight-layer-thick slab model along the [110] direction and a ten-layer-thick slab model along the [100] direction (Fig. S4); further discussions in the context of recent developments. The Supplemental Material includes Refs. [41–43,59,63–68].
[63] A. Siegel, K. Parlinski, and U. D. Wdowik, Phys. Rev. B **74**, 104116 (2006).
[64] T. Hyart, R. Ojajarvi, and T. T. Heikkila, arXiv:1709.05265.
[65] T. Bzdusek, Q. Wu, A. Ruegg, M. Sigrist, and A. A. Soluyanov, Nature (London) **538**, 75 (2016).
[66] R. Yu, Q. S. Wu, Z. Fang, and H. M. Weng, Phys. Rev. Lett. **119**, 036401 (2017).
[67] T. Hyart and T. T. Heikkila, Phys. Rev. B **93**, 235147 (2016).
[68] X. Feng, C. M. Yue, Z. D. Song, Q. S. Wu, and B. Wen, arXiv:1705.00511.
[69] H. Weng, X. Dai, and Z. Fang, J. Phys. Condens. Matter **28**, 303001 (2016).
[70] C. Fang, H. Weng, X. Dai, and Z. Fang, Chin. Phys. B **25**, 117106 (2016).
[71] S. Sur and R. Nandkishore, New J. Phys. **18**, 115006 (2016).